

# Appendix: Additional Experimental Results

Paper Authors

July 18, 2025

## A Additional Results for Different Harmonic Configurations

This appendix presents comprehensive results for all tested harmonic configurations, demonstrating the non-monotonic relationship between harmonic count and solution accuracy. Each configuration was trained using the identical two-phase optimization strategy described in the main text.

### A.1 Three-Dimensional Solution Visualizations

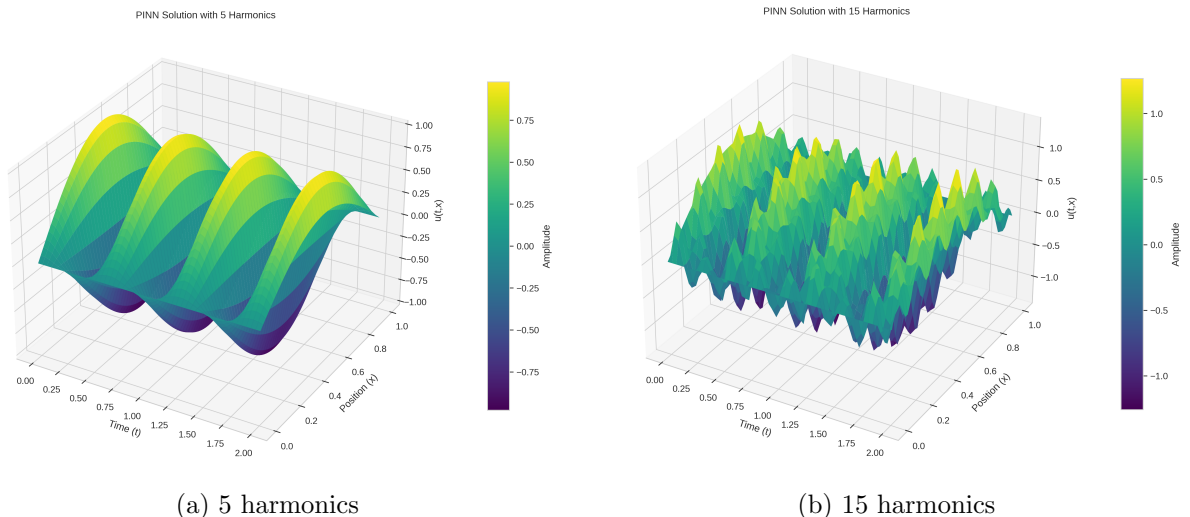


Figure 1: Three-dimensional solution profiles for 5 and 15 harmonics, showing the dramatic degradation in accuracy beyond the optimal configuration.

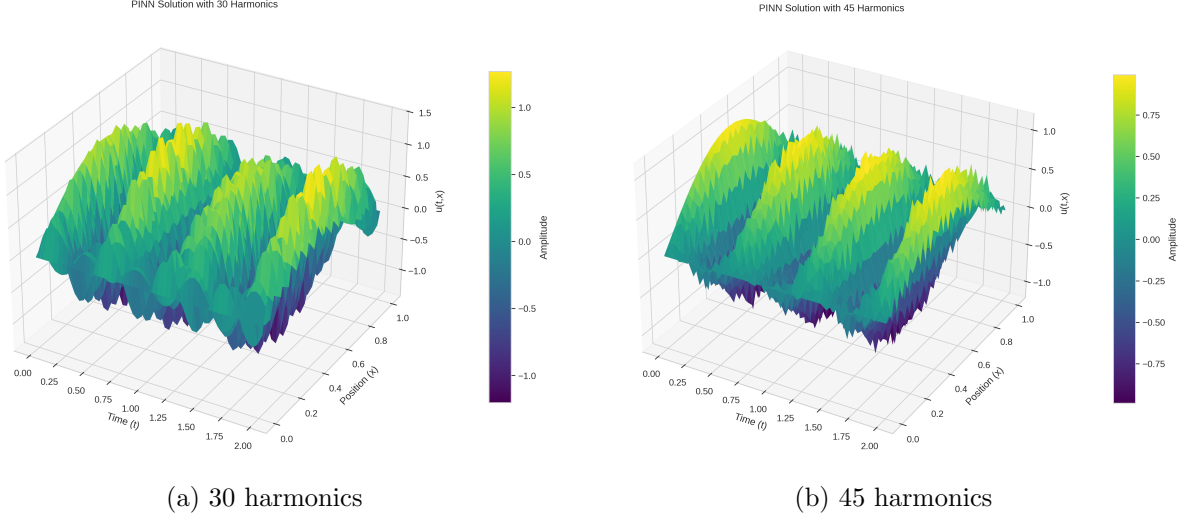


Figure 2: Higher harmonic configurations (30 and 45) demonstrate significant accuracy degradation due to optimization challenges in high-dimensional parameter spaces.

## A.2 Error Distribution Analysis

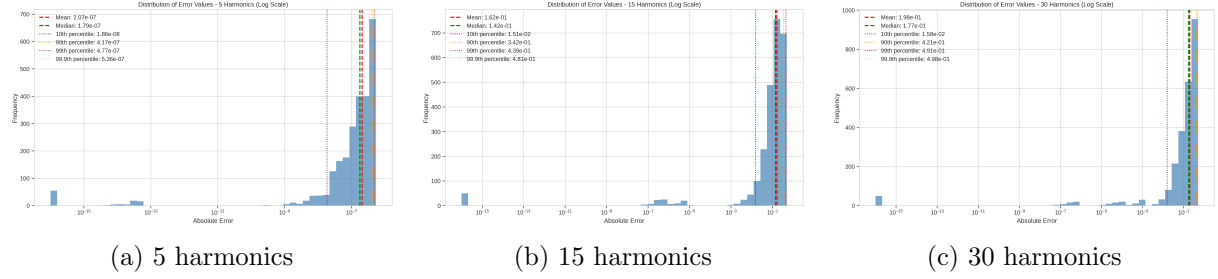


Figure 3: Spatial error distributions for different harmonic configurations, revealing how error patterns change with model complexity.

## A.3 Training Dynamics

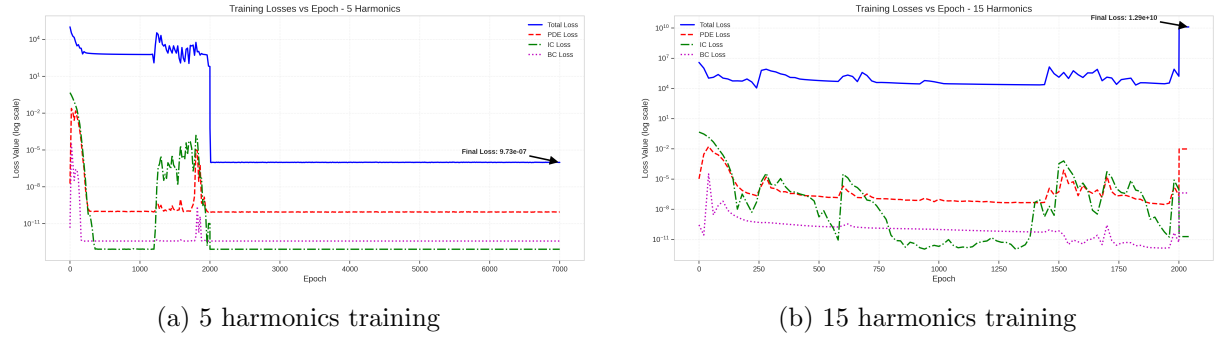


Figure 4: Training loss evolution for suboptimal configurations, showing instabilities and convergence difficulties for higher harmonic counts.

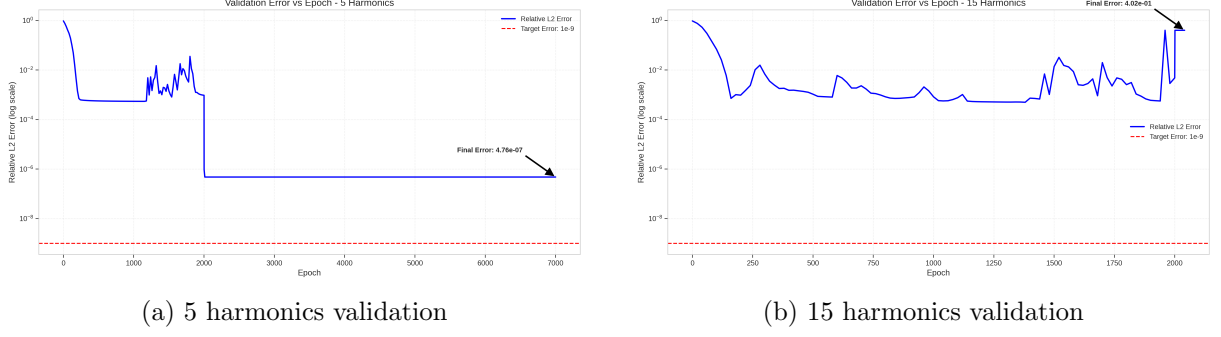


Figure 5: Validation error evolution demonstrating the generalization capabilities across different harmonic configurations.

#### A.4 Beam Deflection Analysis

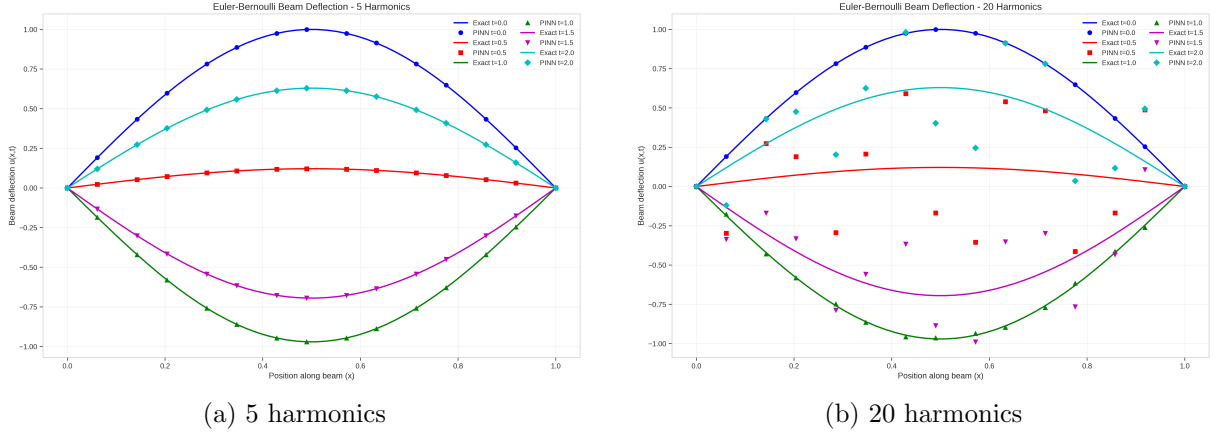
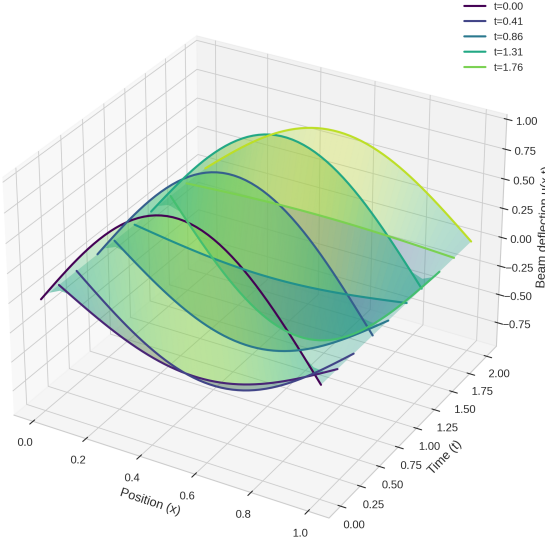


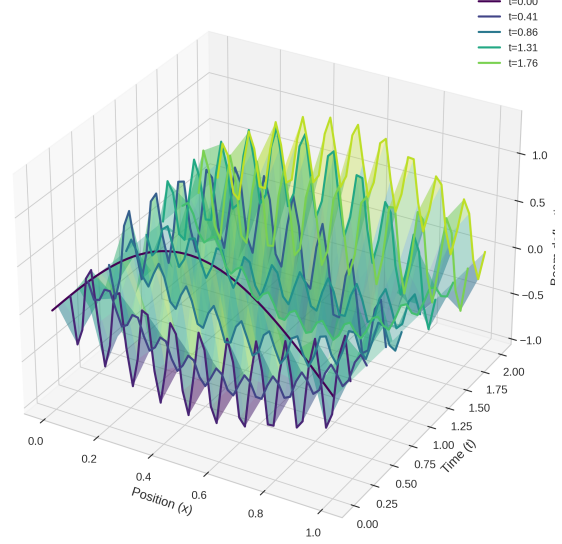
Figure 6: Euler-Bernoulli beam deflection profiles at different time instances, comparing low and moderate harmonic configurations.

Euler-Bernoulli Beam Vibration - 5 Harmonics



(a) 5 harmonics 3D view

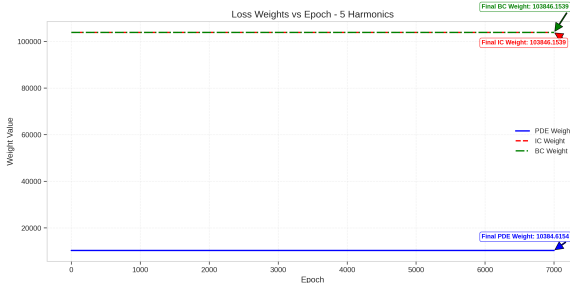
Euler-Bernoulli Beam Vibration - 20 Harmonics



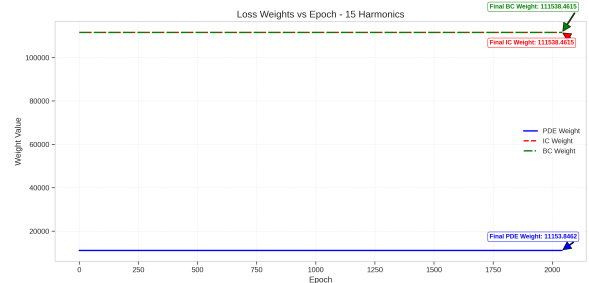
(b) 20 harmonics 3D view

Figure 7: Three-dimensional beam vibration patterns showing the spatiotemporal evolution for different harmonic configurations.

## A.5 Adaptive Weight Evolution



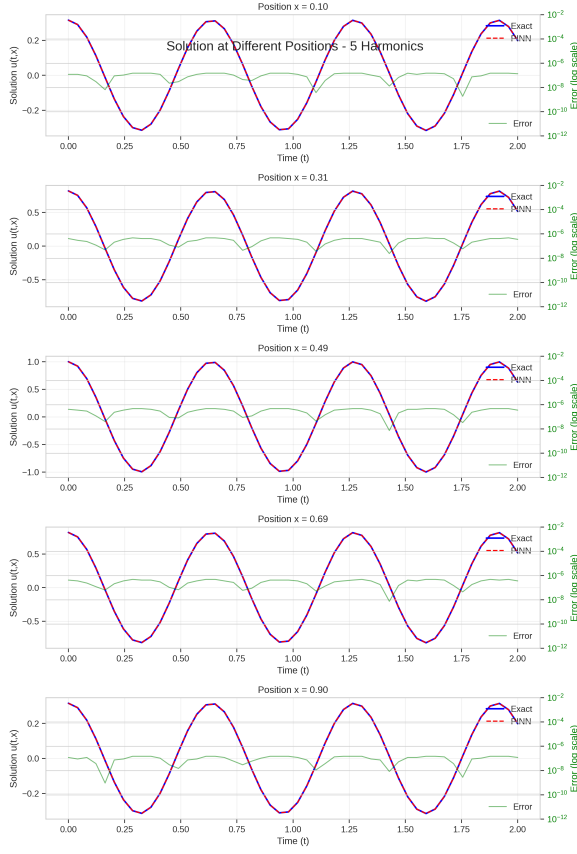
(a) 5 harmonics



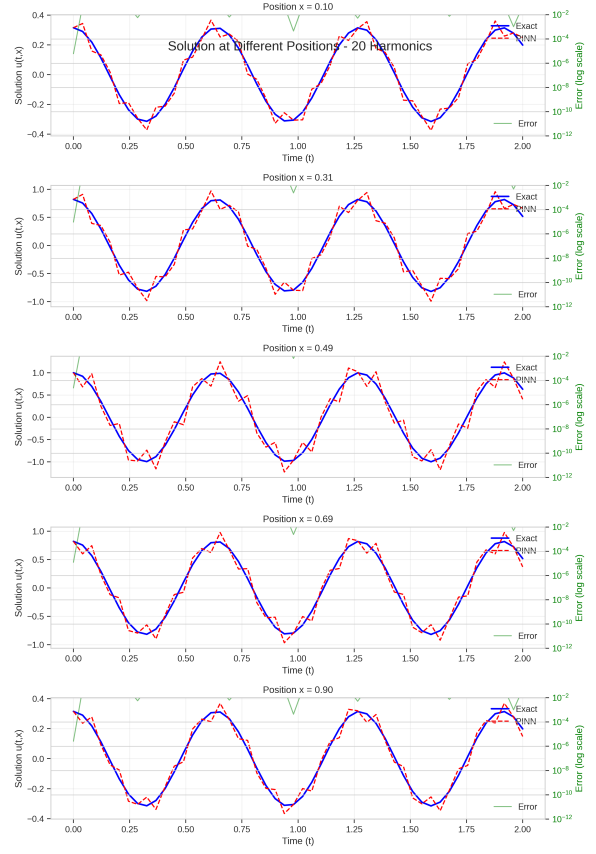
(b) 15 harmonics

Figure 8: Evolution of adaptive weight factors during training for different harmonic configurations, showing how the optimization balances competing loss components.

## A.6 Solution Slice Comparisons

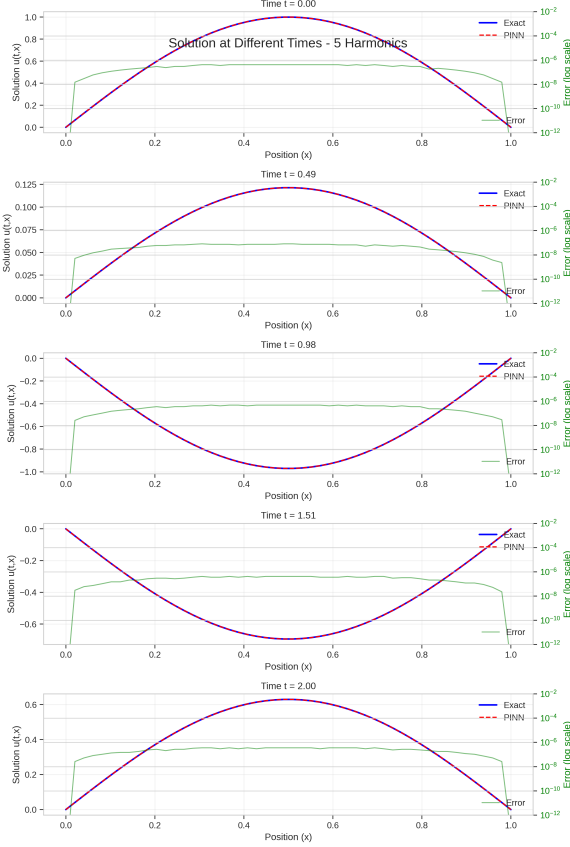


(a) Spatial slices - 5 harmonics

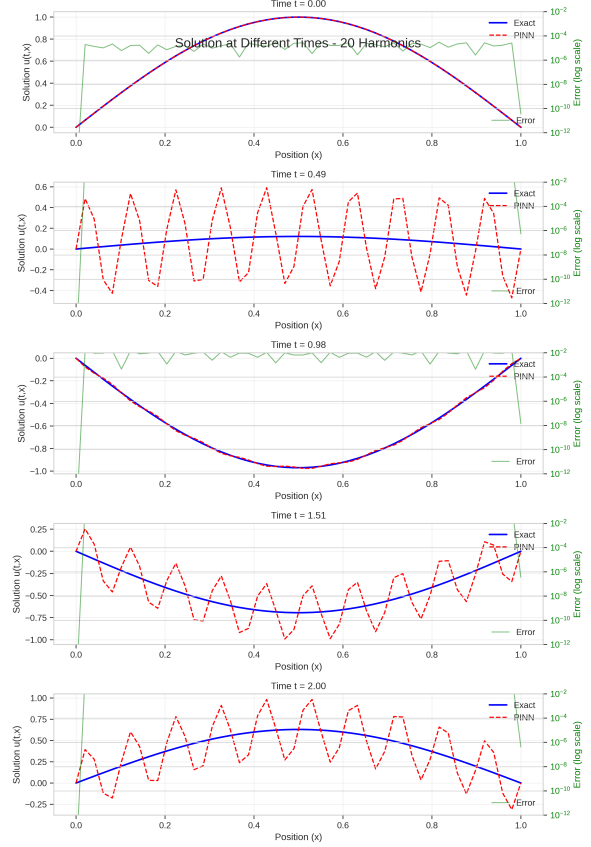


(b) Spatial slices - 20 harmonics

Figure 9: Spatial solution profiles at fixed time points, demonstrating accuracy variations across different harmonic configurations.



(a) Temporal slices - 5 harmonics



(b) Temporal slices - 20 harmonics

Figure 10: Temporal evolution at fixed spatial locations, showing how different harmonic counts affect time-dependent accuracy.

## A.7 Comprehensive Error Comparison

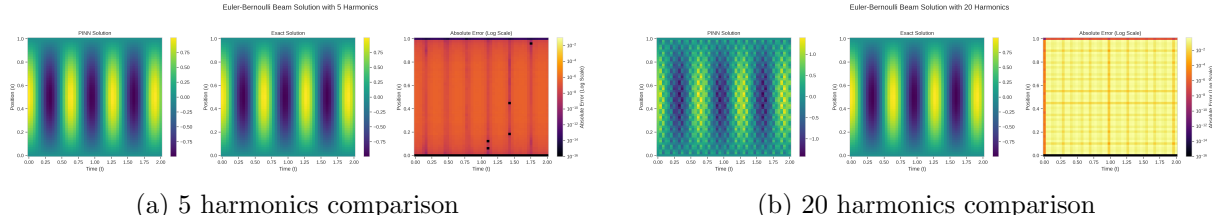


Figure 11: Direct comparison between PINN predictions, exact solutions, and absolute errors for representative harmonic configurations.

The comprehensive results presented in this appendix confirm the optimal performance at 10 harmonics. The degradation observed for higher harmonic counts stems from: (1) increased parameter space dimensionality leading to more complex optimization landscapes, (2) overfitting to training data despite physics-informed regularization, and (3) numerical instabilities in computing high-order derivatives for numerous frequency components. These findings underscore the importance of architectural design choices in achieving ultra-precision solutions for physics-informed neural networks.

## B Complete Experimental Results

This section presents all additional experimental results not shown in the main text, providing a comprehensive view of the model's performance across all tested configurations.

### B.1 3D Error Visualizations

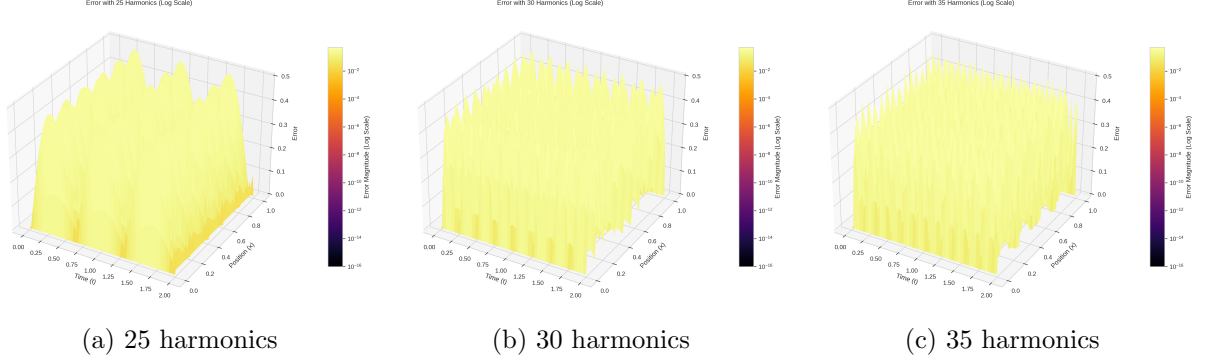


Figure 12: Three-dimensional error surfaces for mid-range harmonic configurations showing the transition from acceptable to degraded accuracy.

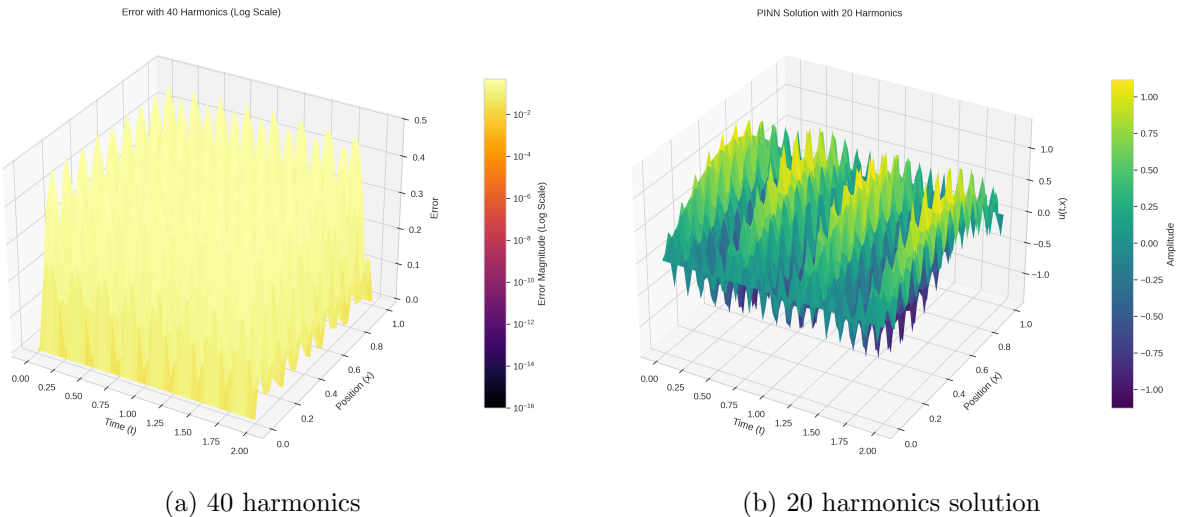


Figure 13: High harmonic error surface and intermediate harmonic solution profile.

## B.2 Additional 3D PINN Solutions

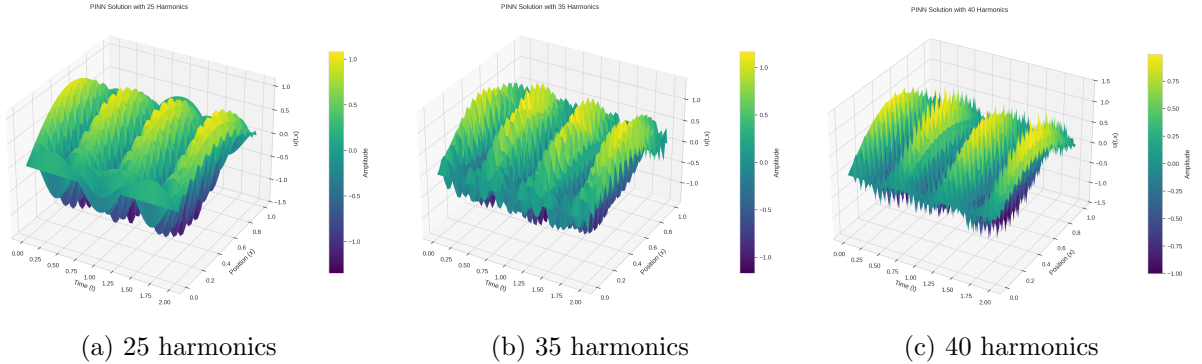


Figure 14: Three-dimensional PINN solutions for additional harmonic configurations.

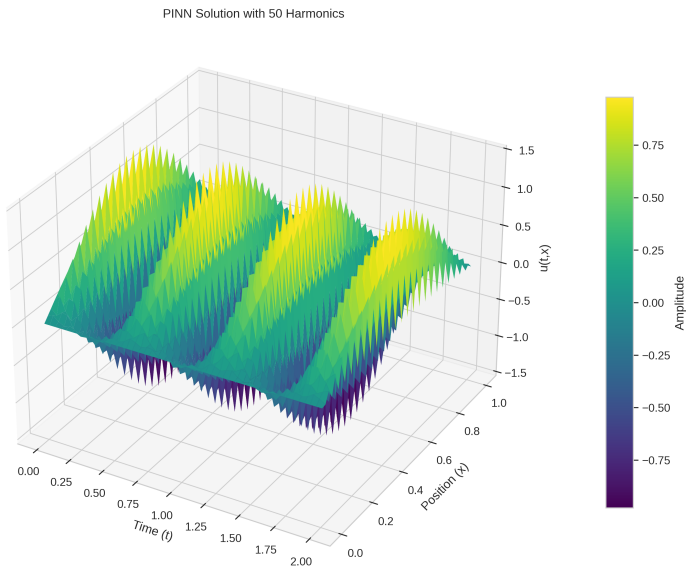


Figure 15: PINN solution with 50 harmonics showing severe degradation in solution quality.

### B.3 Complete Spatial Slice Analysis

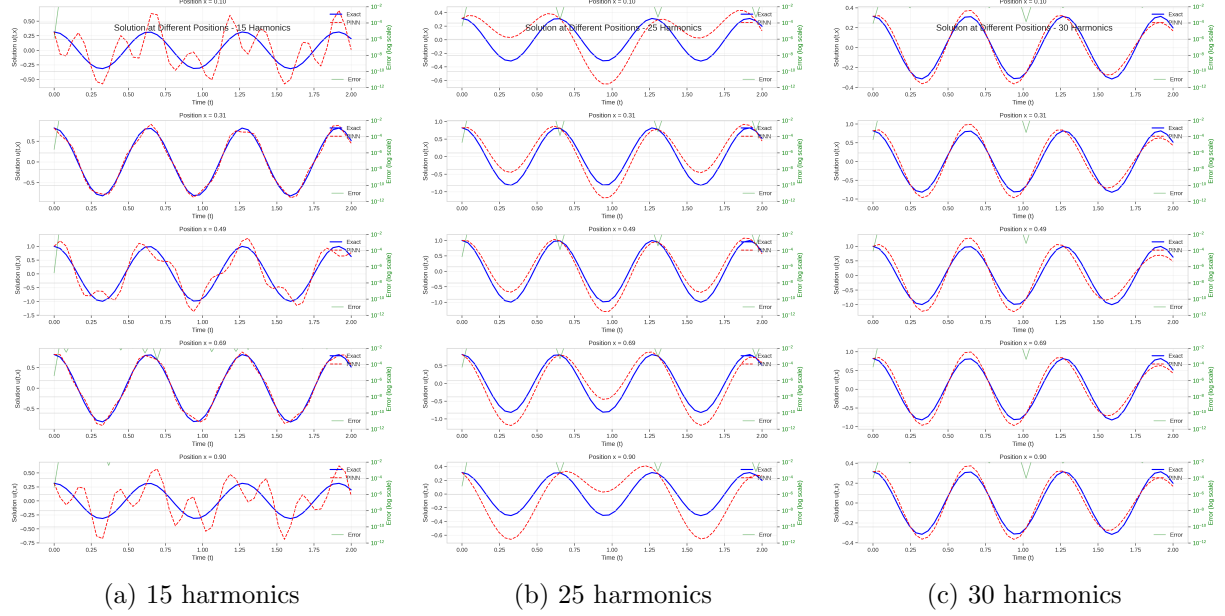


Figure 16: Spatial solution profiles at fixed time points for mid-range harmonic counts.

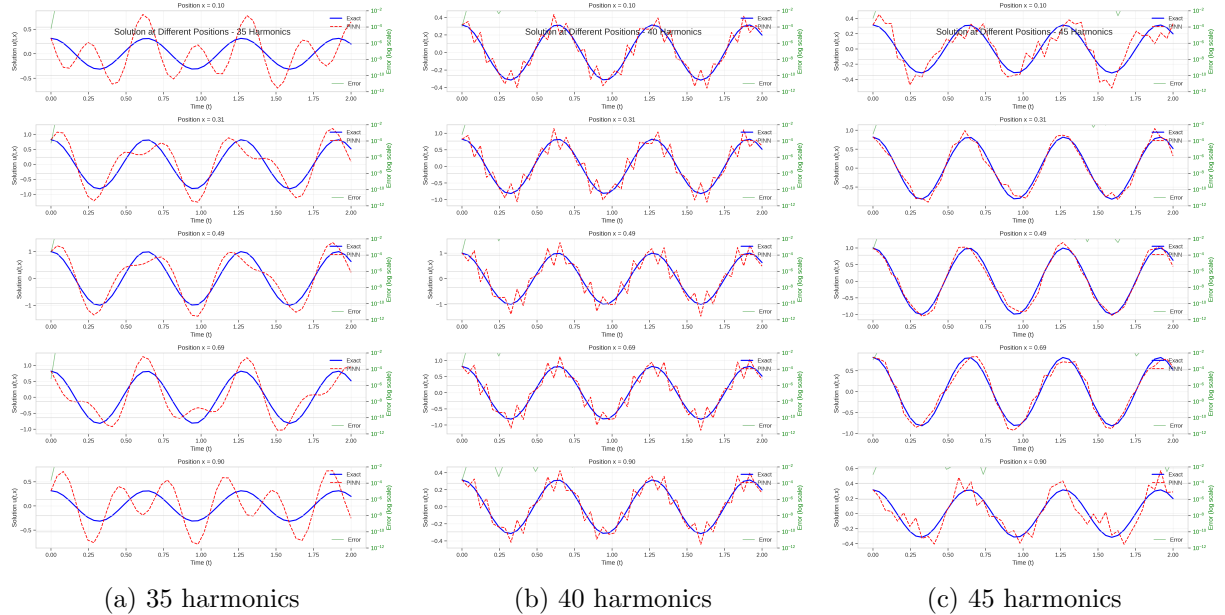


Figure 17: Spatial profiles for high harmonic configurations demonstrating increasing inaccuracy.

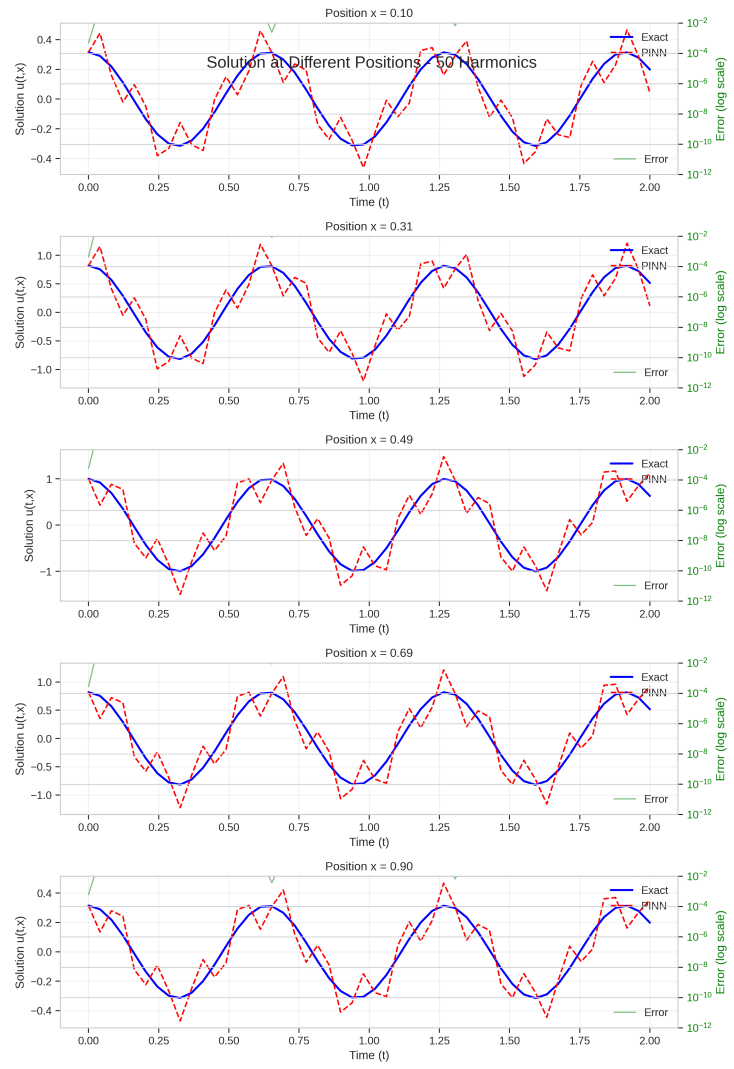


Figure 18: Spatial slices for 50 harmonics showing the most severe accuracy degradation.

## B.4 Complete Temporal Slice Analysis

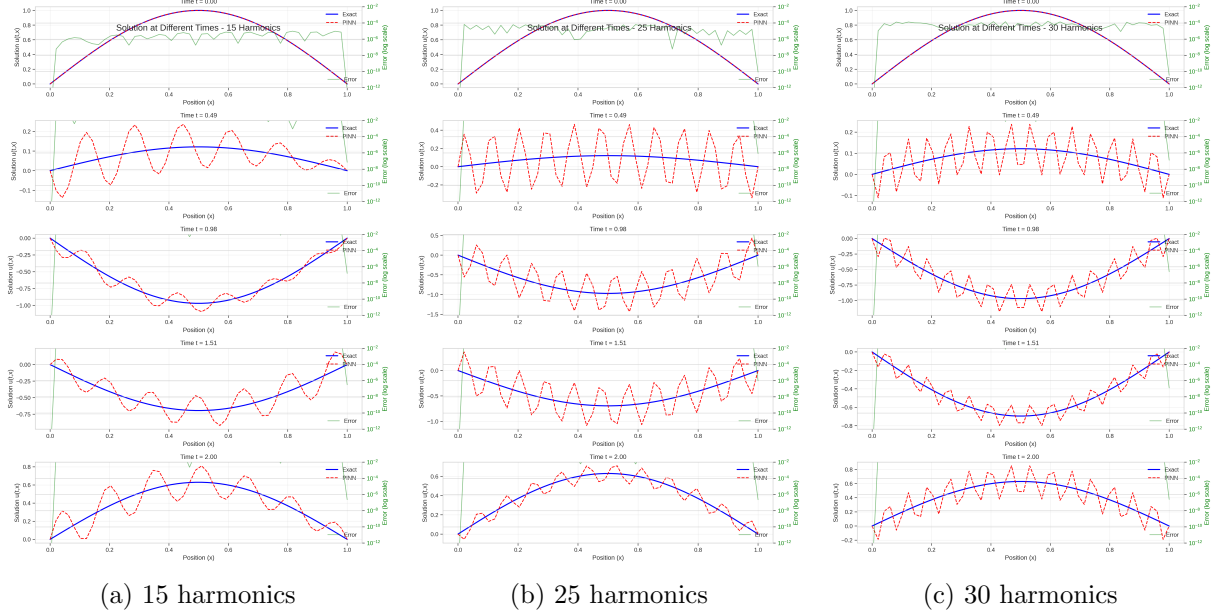


Figure 19: Temporal evolution at fixed spatial locations for mid-range configurations.

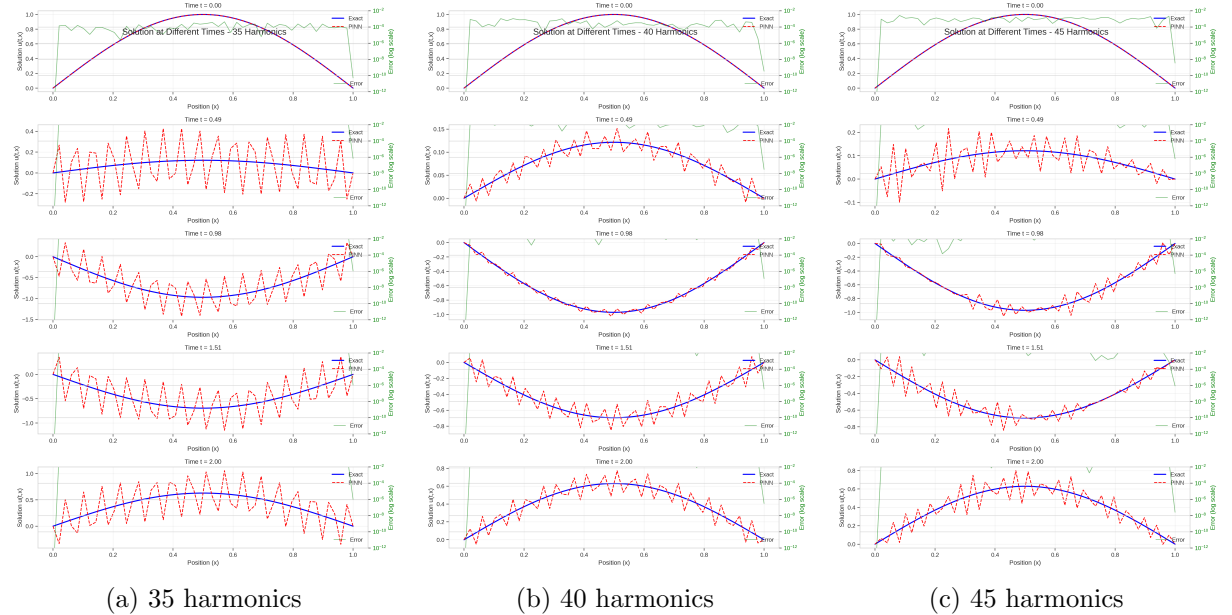


Figure 20: Temporal profiles showing progressive degradation with increasing harmonic count.

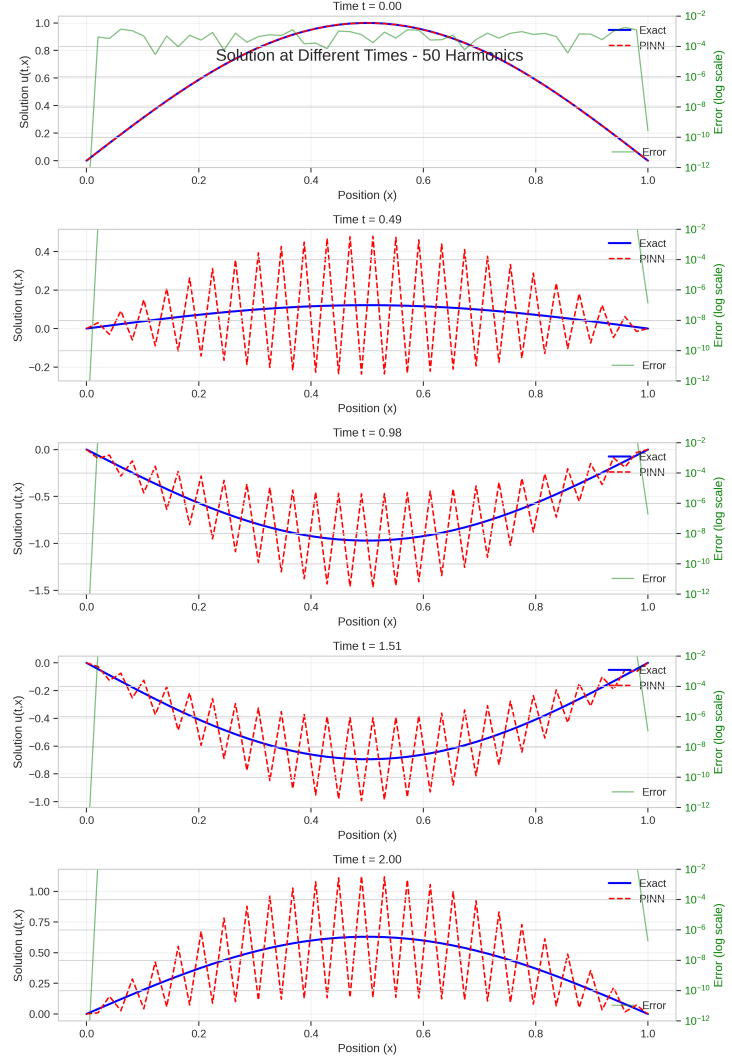


Figure 21: Temporal slices for 50 harmonics configuration.

## B.5 Complete Training Loss Evolution

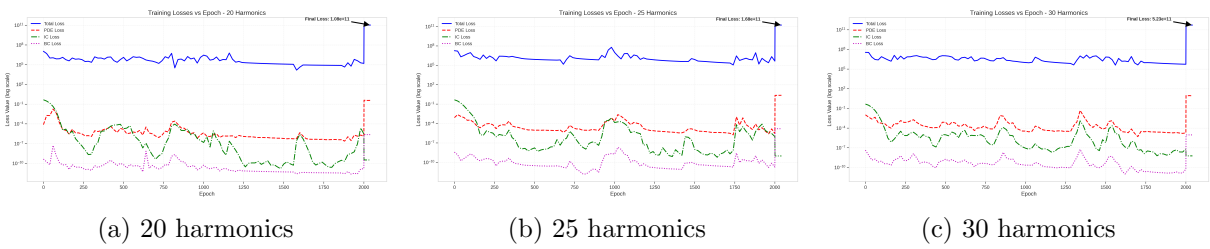


Figure 22: Training loss evolution for mid-range harmonic configurations.

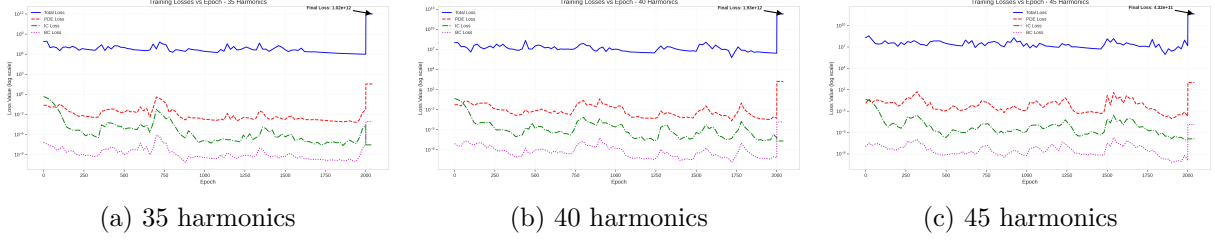


Figure 23: Training dynamics for high harmonic counts showing increased instability.

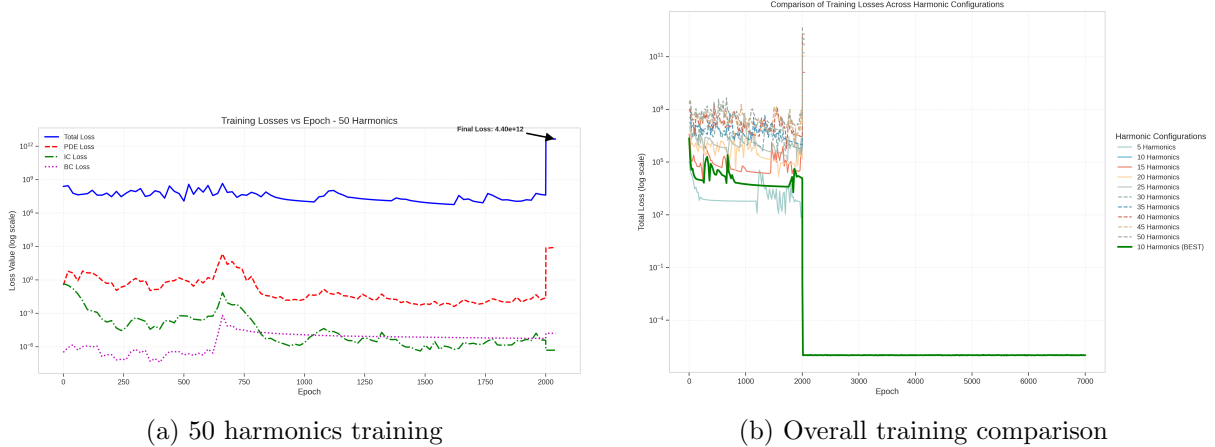


Figure 24: Training loss for maximum harmonic count and comparative overview.

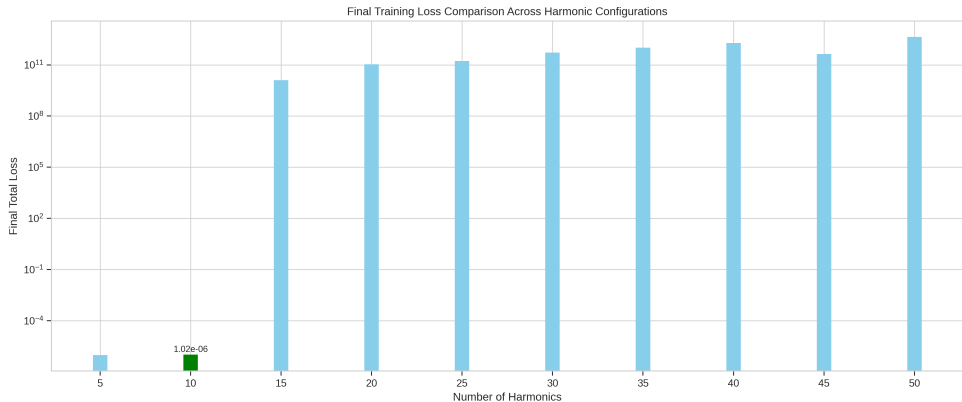


Figure 25: Final training loss comparison across all harmonic configurations.

## B.6 Complete Validation Error Analysis

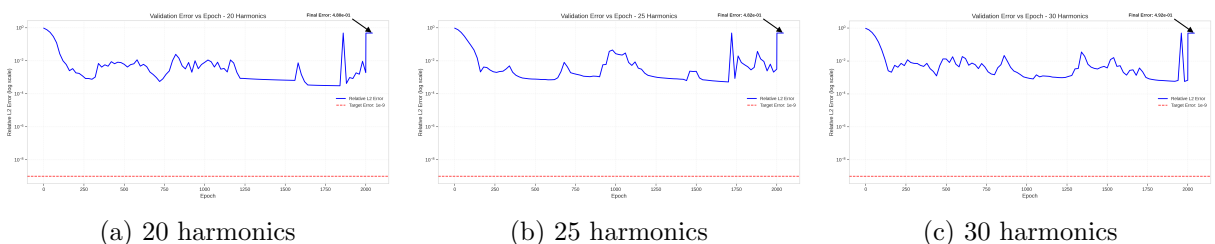


Figure 26: Validation error evolution for mid-range configurations.

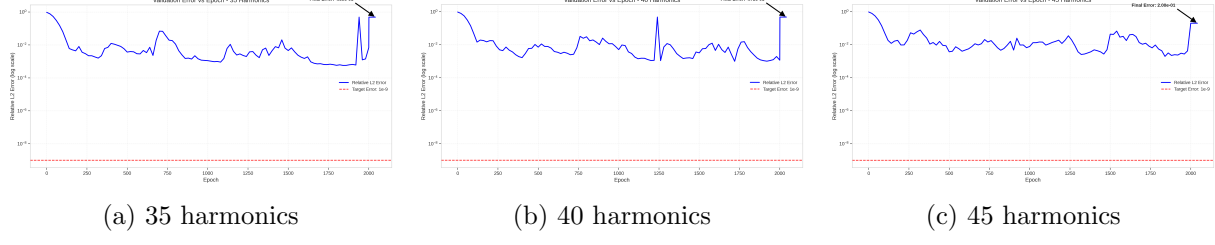


Figure 27: Validation performance for high harmonic configurations.

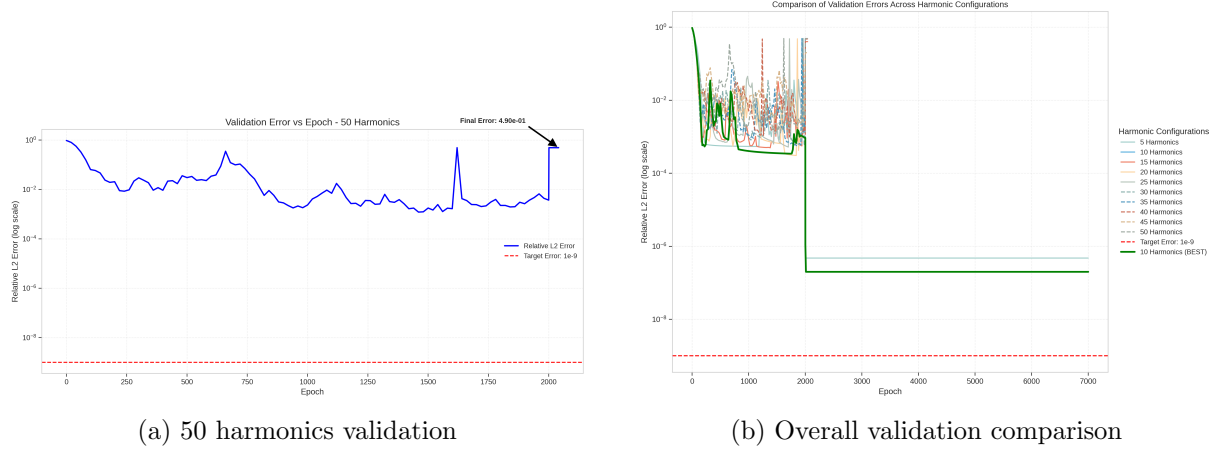


Figure 28: Validation error for maximum harmonic count and comparative overview.

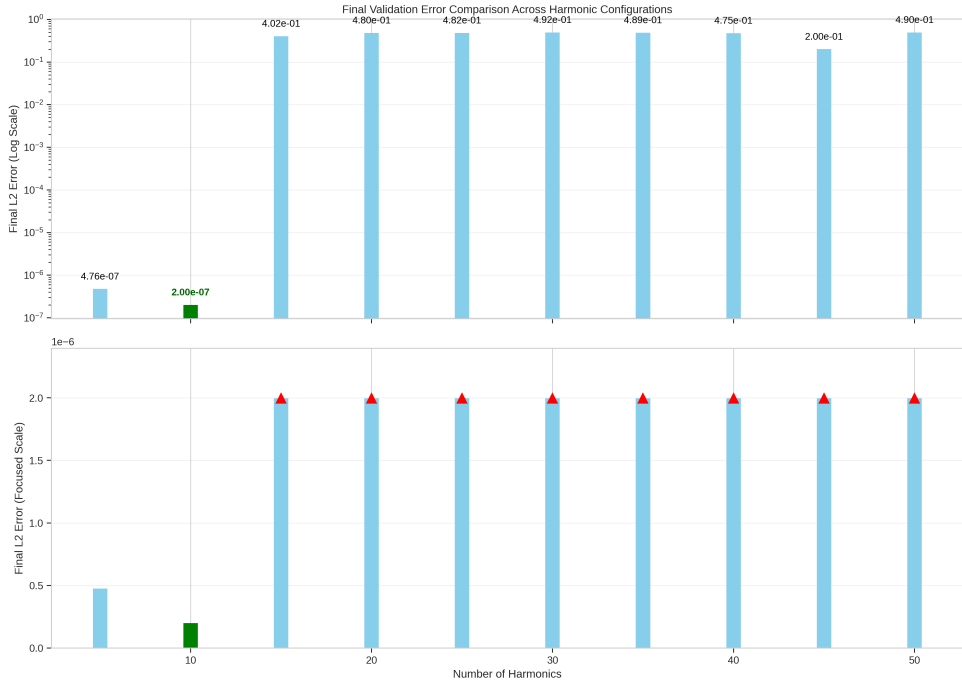


Figure 29: Final validation error comparison highlighting the optimal 10-harmonic configuration.

## B.7 Complete Adaptive Weight Evolution

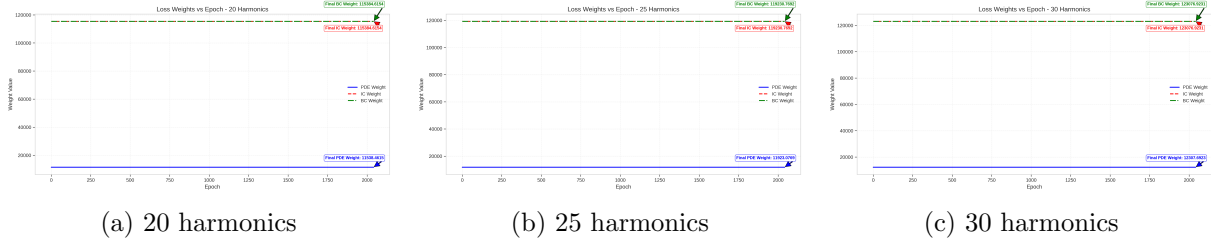


Figure 30: Adaptive weight factor evolution for mid-range configurations.

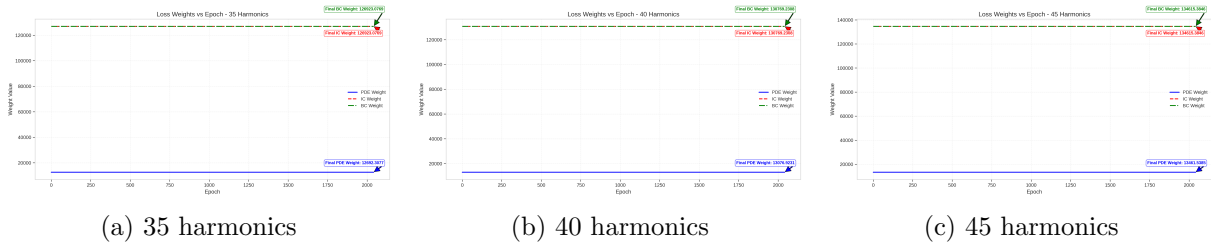


Figure 31: Weight balancing dynamics for high harmonic configurations.

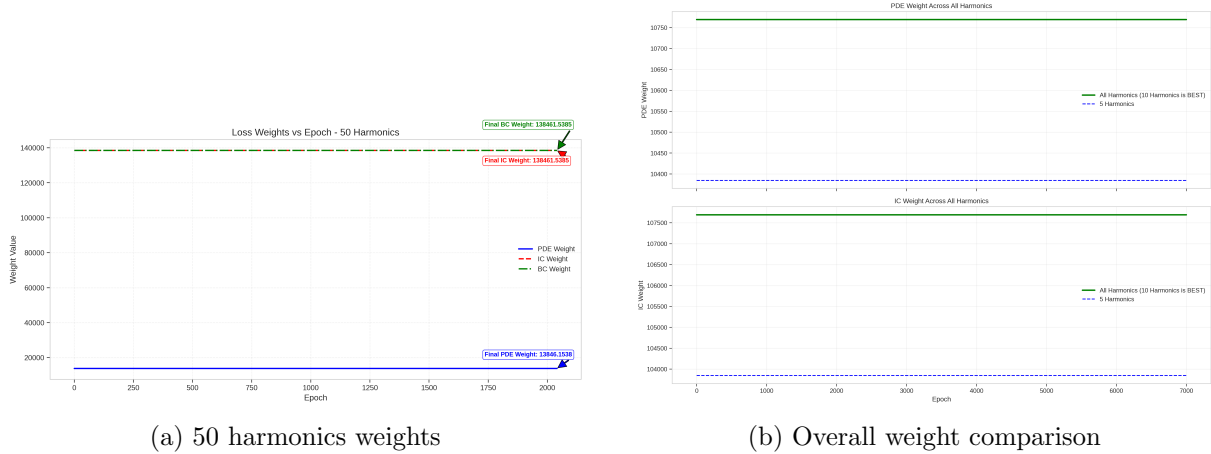


Figure 32: Adaptive weights for maximum harmonic count and comparative analysis.

These comprehensive results provide complete documentation of all experimental configurations tested in our study. The systematic progression from optimal (10 harmonics) to severely degraded (50 harmonics) performance illustrates the critical importance of architectural choices in physics-informed neural networks for high-order PDEs.